Thermal-aware Synthesis of Integrated Photonic Ring Resonators

Christopher Condrat
Calypto Design Systems
chris@g6net.com

Priyank Kalla
ECE Dept., Univ. of Utah
kalla@ece.utah.edu

Steve Blair
ECE Dept., Univ. of Utah
blair@ece.utah.edu

***Abstract*—Photonic ring-resonators are key components of many on-chip optical-interconnect wavelength division multiplexing (WDM) network architectures. Thermal interactions between on-chip heat-sources and ring resonators pose significant operational and integration challenges, as these devices are extremely sensitive to temperature-induced changes in refractive index. Contemporary literature proposes active compensation for such refractive index variations (e.g. carrier-injection based tuning and/or WDM channel remapping); however, these are costly in terms of power and area. This paper presents a thermal-aware synthesis approach for ring-resonator compensation. We show how ring-resonators are analyzed in the presence of external thermal gradients, and employ a *perturbation analysis* to derive an equivalent, trimming-enabled, ring-resonator design. Our methodology produces a design-template that can be used to compensate for thermal variations through modifications to the waveguide's geometric structure. This approach complements active compensation techniques, and the synthesis is compatible with contemporary lithographic methods. Using this approach, we perform design space exploration with respect to variations to the waveguide structure and their effect on the range and precision of thermal compensation.**

1. Introduction

Multi-core processor systems with network-on-chip architectures are fast becoming the norm in VLSI system integration. As these systems introduce greater levels of parallelism at the system level, the need for high-speed, high-bandwidth communications becomes a critical factor in overall system operations. The limitations of VLSI interconnect scaling such as increasing resistivity, low bandwidth, cross-talk, etc., has led researchers in industry and academia to investigate *complementary* technologies — one of which is integrated optics: to enable fast, long-distance (chip scale), low-power and high-bandwidth communications [1]. Silicon-based integrated optics — dubbed *Silicon Photonics* — are well positioned to play an important role in such communication fabrics, providing a high-bandwidth, high-fidelity transport layer for inter- and intra-chip communications.

A key component of many optical network architectures is wavelength division multiplexing (WDM). Consider a high-level overview of a WDM network depicted in Fig. 1(a). In an optical WDM network, channels of data are assigned to specific wavelengths of light. Wavelength-tuned multiplexing devices — *integrated photonic ring resonators* in this case — are used to modulate this light, enabling signals (data) to be injected into the waveguide. The light is then routed through the communications fabric. At the endpoints, demultiplexing devices (again, ring-resonators) select for particular wavelengths of light and the signals they carry. This light is then detected at the end-points by an optical receiver.

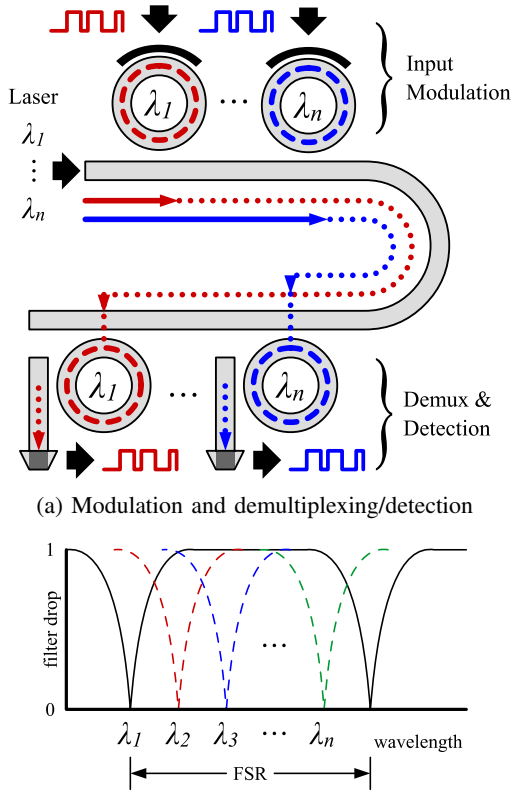

(a) Modulation and demultiplexing/detection

(b) Channel wavelengths within the FSR of a WDM ring resonator

Fig. 1: WDM network overview and channel assignments

At the core of these optical WDM network architectures is the photonic ring resonator [2]. Ring resonators are used to modulate/multiplex as well as filter (demultiplex) signals on waveguides as depicted in Fig. 1(a). This device is particularly suited for this application because of its high degree of wavelength selectivity and small footprint. This enables ring-resonator-based WDM systems to support large numbers of channels on the same photonic waveguide.

The filtering response of a ring resonator is periodic with respect to wavelength. Qualitatively, the wavelength range between resonant (filter) peaks is the free spectral range (FSR).

The FSR, in conjunction with the filtering characteristics of the rings, sets the upper limit on the number of channels. In general, the smaller the ring, the greater the FSR, as limited by manufacturability and the waveguide's minimum radius of curvature. The ring resonators of a WDM network are usually designed with the same FSR to allow consistent channel spacing without overlap. This channel-wavelength assignment is depicted in Fig. 1(b).

A. Integration Challenges

A major challenge in using ring-resonators for mux/demux operations is their extreme sensitivity to refractive index changes [2]. *Process variation, geometric variations, and also thermal effects can shift a ring's response off its designed resonant wavelength.* Silicon-based ring resonators are especially susceptible to temperature-induced changes to refractive index (n) due to silicon's large thermo-optic coefficient of $dn/dT = 1.86 \times 10^{-4}/^{\circ}K$. Resonance shifts of $0.1nm/^{\circ}K$ have been reported, causing high bit-error-rates (BERs) for a ΔT of a few degrees [3].

In systems that integrate silicon photonic WDM networks, as those depicted in Fig. 2(a), the underlying electronic layer (computational units/cores) will act as heat sources within the chip. These temperature hot-spots will generate a thermal gradient across the optical routing substrate. This, in turn, will cause temperature-induced changes to the refractive index of the photonic layer, *causing the rings to fall out of resonance*. Furthermore, the locality of heat sources means that different rings will be subjected to different temperature conditions such as depicted in Fig. 2(b). Such external thermal gradients pose significant operational challenges to ring-resonator-based WDM networks.

Contemporary literature proposes *active compensation* for such refractive index variations: 1) Using microheaters embedded around the rings, or overlaid on the oxide cladding, to effect a temperature-induced change in the refractive index [5]; 2) Tuning by carrier-injection that applies a DC bias to the ring. Highly doped P and N regions are used to form a P-i-N junction around the ring, and free-carriers are injected into (conversely, extracted from) the rings to cause carrier concentration induced refractive index changes [6], [7].

Such techniques are costly in terms of power, area, and restrictive in terms of tuning range. Microheater-based tuning is very slow, cumbersome to tune precisely, consumes large amount of power (*e.g.* $50mW$ for $16nm$ tuning range per device [8]), and it exacerbates the already strained energy-density on chip. DC-bias based tuning has limited range (of the order of $8.7V \times 0.017nm/V/0.088nm/^{\circ}C$ [6]). These techniques require outside energy and feedback to prevent resonance wavelength drift and offset, negatively impacting power and area.

B. Our Contribution: Thermal-Aware Synthesis

We present a *thermal-aware synthesis approach for ring-resonator compensation.* This approach utilizes a template-based ring-resonator design that enables process-compatible (re)synthesis to compensate for pre-computed average- or worst-case thermal gradients. One can assume that an average-case or worst-case workload characterization is known for the multiprocessor system, from which the temperature characterization over the optical chip can be determined utilizing techniques such as in [9]. Such thermal data is provided as an external constraint to our technique.

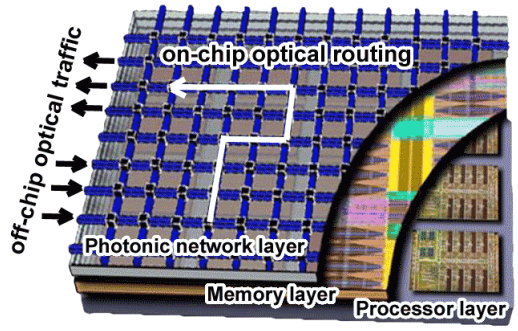

(a) Photonic routing layer in an integrated chip design. *Image credit: IBM* [4]

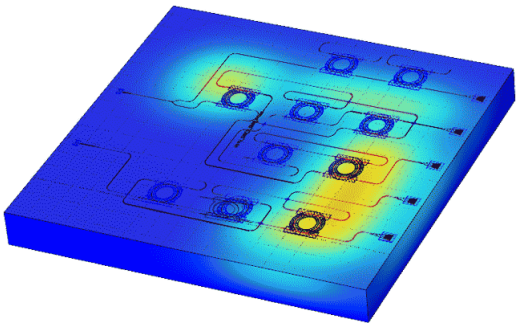

(b) On-chip heat sources creating thermal gradients across an optical substrate

Fig. 2: Integration of ring-resonator networks.

Thermal gradients are indeed data-dependent. Therefore, some dynamic compensation mechanism is certainly needed. However, given a large temperature variation on chip, it may not be feasible to perform ring-resonator tuning purely dynamically. This is because: 1) a limited tuning range may preclude techniques from being utilized given a large wavelength shift [3], [5], [6] and 2) tuning power requirement may be too great [10] to make it practical. For such reasons, static tuning (around an average-case thermal gradient) along with lower-range dynamic tuning will be needed.

In this work, we perform resonance analysis of ring-resonators and identify geometric parameters that can be modified for the purpose of thermal compensation. Exploiting these parameters, our (re)synthesis methodology generates a *parameterized design template* for racetrack-style ring-resonators that can compensate for different temperature conditions. Thermal variations are compensated by engineering a perturbation in the ring waveguide profile — in effect countering thermal/material changes via geometric changes. While perturbations in photonic structures are well-understood and widely employed for coupling in resonant cavities, the novelty of this approach is its use as a *thermal compensation*

mechanism. Finally, we demonstrate how this thermal-aware (re)synthesis methodology can be automated, and where design space exploration can be performed with respect to the range and precision of thermal compensation.

Our proposed thermal-aware synthesis is an attractive option because modifications to devices can be performed without special processing steps, materials, or relying purely on active compensation. *While this approach is not an alternative to active tuning, it complements active tuning.* Some amount of active tuning will certainly be required; however, our redesign ensures a smaller tuning range, thereby reducing the required power/heat for carrier injection or microheater based tuning.

Paper organization: Section 2 describes contemporary work in ring resonator compensation. Section 3 describes the ring resonator model and operational parameters. In Section 4, we describe our compensation technique using a perturbation analysis of the waveguide structure. This is followed by our template-based synthesis methodology, and a demonstration using a ring resonator design under various temperature conditions and design parameters (Section 5). Section 6 concludes this paper.

2. Contemporary Work

Active compensation (tuning) utilizes external effects to change the optical properties of materials. For SOI ring resonators, active tuning is usually implemented via microheaters [5] — exploiting silicon's relatively large thermo-optic coefficient. Tuning can also be performed by using carrier injection, by applying a DC-bias to the ring [6]. Operating system scheduling techniques have also been proposed to control dynamic compensation [7]. In all such active compensation methods, outside energy and feedback are required to prevent resonance wavelength drift and offset. [7]

Channel-remapping approaches [11] have been proposed as a means to reduce active power. These approaches reassign WDM channels to different rings depending on their perturbed resonance conditions and require active tuning power. The drawback to this approach is that a larger number of rings are necessary to enable channel remapping, and rings may conflict should their filtering response be similar. In [12], thermal-aware global routing for optical WDM networks are presented; however, it does not address ring resonator compensation.

Permanent compensation can be achieved by manipulating the optical properties of a waveguide's materials — i.e. "trimming." Trimming is often performed by affecting the waveguide's cladding layer through stress or additional material layers [13], [14], or by introducing materials that counteract the thermo-optic coefficient of silicon, such as polymers on narrowed waveguides [15]. Such *athermal* design methods require additional materials and lithographic processes that increase the cost and complexity of fabrication. In addition, materials such as polymers on narrowed waveguides can affect mode confinement, disallowing sharp bends [2].

3. Ring Resonator Modeling

Optical ring resonators are wavelength filtering devices with a notch-filter-type response curve centered around a resonant wavelength. These devices rely on a resonance condition, which causes light within the ring to destructively interfere with light on the coupling waveguides. Alternatively, with two straight waveguides coupled to a single ring, a ring resonator can be used to couple specific wavelengths into or out of a waveguide in a 2x2-switch type operation.

Consider the ring resonator structure depicted in Fig. 3(a), where a ring of radius r is coupled to a straight waveguide. The coupler is assumed to be symmetrical, and also lossless, implying that the coupling coefficient K is related to the transmission coefficient t by:

$$K^2 + t^2 = 1 \tag{1}$$

The ring has an overall length of $L = 2\pi r$, and round-trip loss coefficient α.

A functional model (block diagram) for the ring resonator structure is depicted in Fig. 3(b). The electric field amplitude E_{b_2} is the sum of the input electric field E_{a_1} coupled into the ring with coefficient K, and the round-trip feedback of the ring E_{a_2} coupled back into the ring with coefficient t. Likewise, E_{b_1} is the sum of the t-coupled input signal E_{a_1} and the K-coupled signal E_{a_2}. These are expressed as:

$$E_{b_2} = \frac{-jKE_{a_1}}{1 - t\alpha e^{-j\phi}} \tag{2}$$

$$E_{a_2} = E_{b_2}\alpha e^{-j\phi} \tag{3}$$

$$E_{b_1} = tE_{a_1} - jKE_{a_2} \tag{4}$$

where $\phi = \beta L$ is the phase produced by the round-trip traversal of the ring from b_2 to a_2. The $-j$ factor attached to K is the result of coupling from one waveguide to another: the latter signal always lags the former by a 90° phase shift.

Combining Eqns. (2)–(4) and squaring the result to determine power results in:

$$\frac{P_{b_1}}{P_{a_1}} = \left|\frac{E_{b_1}}{E_{a_1}}\right|^2 = \frac{\alpha^2 + |t|^2 - 2\alpha|t|\cos(\phi)}{1 + \alpha^2|t|^2 - 2\alpha|t|\cos(\phi)} \tag{5}$$

The value of Eqn. (5) drops to zero (0) when two conditions are met: 1) critical coupling, and 2) the resonance condition for the ring. The first condition, *critical coupling,* occurs when losses in the ring α equal those of the transmission coefficient, i.e. $\alpha = |t|$. Ideally, the ring is considered lossless, i.e. $\alpha \approx 1$, implying that $t = 1$ and from Eqn. (1) that $K = 0$. The second condition, denoted the *resonance condition* constrains

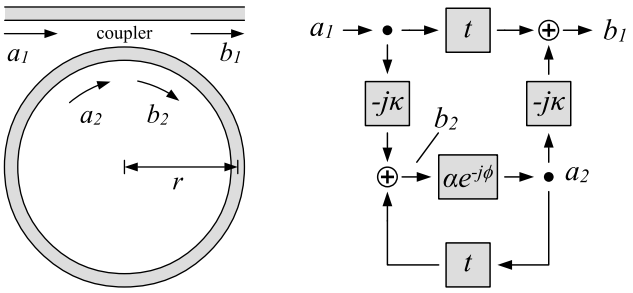

(a) Ring Resonator (b) Block Diagram

Fig. 3: Structure of an Optical Ring Resonator

the round-trip phase of the ring:

$$\phi = \beta \cdot L = 2\pi \cdot m \tag{6}$$

where m is an integer. This causes the term $\cos(\phi) = 1$ and in conjunction with critical coupling $P_{b_1}/P_{a_1} = 0$. The dependence of ϕ on β implies that resonance is wavelength and waveguide (i.e. effective index) dependent. A useful relationship is derived:

$$\beta \cdot L = \frac{2\pi n_{eff}}{\lambda_0} \cdot L = 2\pi \cdot m \quad \Rightarrow \quad n_{eff} \cdot L = m \cdot \lambda_0 \tag{7}$$

where n_{eff} is the effective index of the waveguide and λ_0 is the freespace wavelength of light.

A. Free Spectral Range

As noted earlier, ring resonators have a free spectral range (FSR), the $\Delta\lambda$ between resonance peaks depicted in Fig. 1(b). More formally, the FSR is defined as:

$$\text{FSR} = \frac{\lambda_0^2}{n_g L} \tag{8}$$

where n_g is the dispersion-dependent *group index* of the waveguide:

$$n_g = n_{eff} - \lambda \frac{\partial n_{eff}}{\partial \lambda} \tag{9}$$

For more details on ring resonator design and operation, the reader is referred to [2].

4. Thermal Compensation for Ring Resonators

Consider the racetrack resonator depicted in Fig. 4(a). The resonator is a 4-port structure that facilitates multiplexing/demultiplexing of signals at particular wavelengths. This resonator is operationally the same as a ring resonator as far as total ring length is concerned, but with the benefit that the straight waveguide sections are more easily characterized than the curved sections; we use "ring" to refer to both types of structures.

Optical signals at the *same* wavelength as the ring's resonant wavelength are routed to the *drop*-port; non-resonant wavelengths pass to the *through*-port. This operation can be used to both couple signals onto waveguides or off waveguides and is highly dependent on the ring's designed resonant wavelength.

Temperature variations can cause a ring's resonant wavelength shift due to changes in refractive index. We define $n_{eff,0}$ as the effective index of the waveguide in the *absence* of a thermal variation, i.e. $T = T_0$. A change in temperature ΔT results in a change to the effective index due to the thermo-optic properties of the waveguide materials, notably in the waveguide's silicon guiding layer. This change in refractive index, in turn, causes a change to the waveguide's propagation constant.

Let $n_{eff,\Delta T}$ and $\beta_{\Delta T}$ respectively denote the effective index and propagation constant in the presence of a temperature change $T = T_0 + \Delta T$. The change in propagation constant causes the ring to shift out of resonance as governed by Eqn. (6). This shift can be compensated in multiple ways: 1) active compensation using external effects, such as heat, electric fields, etc., 2) material-level compensation, and 3) geometric changes to the device structure or waveguide — as discussed in the previous section. Our emphasis is on manipulations to the geometry of the waveguide structure.

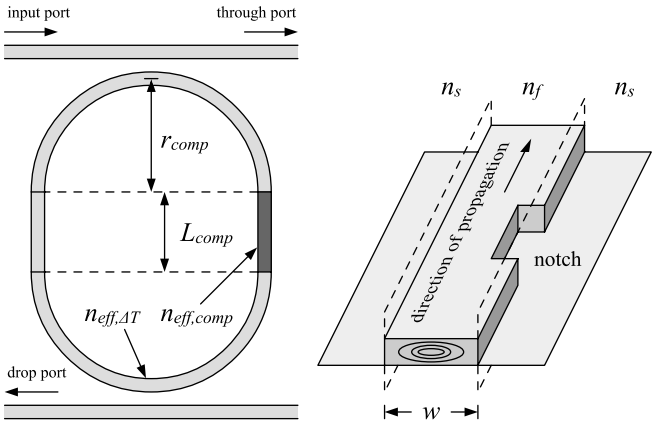

(a) Racetrack (ring) resonator with compensation region

(b) 3D representation of a waveguide with notch; 2D regions of material indexes

Fig. 4: Racetrack (ring) resonator with compensation region

A. Compensation using Ring Length

The racetrack resonator structure in Fig. 4(a) incorporates two compensation regions of length L_{comp} such that $L = 2(\pi r_{comp} + L_{comp})$ satisfies Eqn. (6). By varying the parameter L_{comp}, facilitating a ring-length change, we can compensate for changes in refractive index. Incorporating the above L into Eqn. (7) we have

$$m\lambda_0 = 2(\pi r_{comp} + L_{comp})\left(n_{eff,0} + \frac{dn}{dT}\Delta T\right) \tag{10}$$

where dn/dT is the thermo-optic coefficient of the waveguide structure, which is on order of that of the guiding silicon layer ($\frac{dn}{dT} = 1.86 \times 10^{-4}/^{\circ}K$). Rearranging for L_{comp} gives us:

$$L_{comp} = \frac{m\lambda_0}{2\left(n_{eff,0} + \frac{dn}{dT}\Delta T\right)} - \pi r_{comp} \tag{11}$$

From Eqn. (11) we wish to determine the change in L_{comp} as a function of temperature change. This leads to the expression:

$$\begin{aligned}\Delta L_{comp} &= \frac{m\lambda_0}{2\left(n_{eff,0} + \frac{dn}{dT}\Delta T\right)} - \pi r_{comp} - \left(\frac{m\lambda_0}{2n_{eff,0}} - \pi r_{comp}\right) \\ &= \frac{m\lambda_0}{2}\left(\frac{1}{n_{eff,0} + \frac{dn}{dT}\Delta T} - \frac{1}{n_{eff,0}}\right)\end{aligned} \tag{12}$$

Equation (12) implies that values of ΔT produce small differential quantities, and likewise small changes to ΔL_{comp}. These variations can, however, be multiplied in effect by increasing the ring length through parameter m. For example, consider a ring resonator constructed using a waveguide with dimensions $W \times H = 400$ nm $\times$ 180 nm, with $n_{eff,0} = 1.9065$ at the resonant wavelength $\lambda_0 = 1550$ nm. Evaluating Eqn. (12)

when the waveguide undergoes a change in temperature $\Delta T = 10^{\circ}K$ we have:

$$\Delta L = \frac{m \cdot 1550 \text{ nm}}{2} \cdot \left(\frac{1}{1.9065 + 10^{\circ}K \cdot \frac{1.86 \times 10^{-4}}{^{\circ}K}} - \frac{1}{1.9065} \right) = m \cdot (-0.39620 \text{ nm}) \quad (13)$$

The effect of the temperature change is therefore so small that ring length change must amplify its effects in order for compensation to be effective. Even if we assume (impractically) the lithographic process can fabricate features on order of ≈ 10 nm, the minimum value of m is ≈ 25, implying $L \approx 20.3\mu$m, for compensation at relatively coarse $10^{\circ}K$ increments.

Modifying the ring length has further drawbacks. As observed in Eqn. (8), ensuring precision requires that L must have a minimum length, possibly impacting ring specifications such as the FSR, which is inversely proportional to L. Also, in changing the length of the ring, the dimensions of the entire ring structure (footprint) must be changed, further affecting placement and routing. This approach *does not* lend itself to a template-based methodology. Therefore, we propose a different, more practical, approach to compensation.

B. Compensation using Waveguide Width

The guiding properties of a waveguide are dependent on both materials and geometry of the waveguide profile. As light propagates down a waveguide, variations to this dielectric profile, as a function of length, affects the propagation parameters of guided light within the structure. By introducing *perturbations* to the waveguide structure, a designer can exploit this mechanism to control the transmission and reflection properties of the waveguide. Purposely introduced waveguide perturbations are usually used in the context of creating resonant structures of periodic dielectric variations. For example, structures such as Bragg gratings [16] control for the width and spacing of these periodic perturbations to provide wavelength filtering.

We control for the waveguide *width* for a fixed compensation length (denoted a "notch") in order to introduce a perturbation that enables ring-resonator tuning. This is depicted in a 3D representation of a waveguide in Fig. 4(b). The novelty of this approach is that we can control and tune for round-trip phase within a ring by changing the propagation properties — via the waveguide width — in a short *subsection* of the ring. Also, by controlling for only this subsection of the overall ring length, we have greater control over the phase tuning. This is important for ensuring that waveguide width tuning remains feasible for semiconductor process resolutions.

Finally, for rings of a given resonant wavelength, we construct a single template ring. The resonator template is bound by three conditions: 1) the overall structure and effective index must satisfy the resonance condition Eqn. (6); 2) the compensation region length must minimize reflections to avoid signal loss; 3) variations to the waveguide width must be feasible in current processes. Tuning is performed only by modifying the width of the compensation region without requiring additional resynthesis procedures over the other segments of the ring.

1) Resonance Condition: Satisfying the resonance condition for the ring is implicit, as this ensures that the ring is tuned for a specific wavelength. As the ring is broken down into sections, the phase term for the ring is the integral of the refractive index changes around the ring:

$$\phi = 2\pi m = \int_0^L \beta(z) dz = \beta_{\Delta T} (2\pi r_{comp} + L_{comp}) + \beta_{comp} L_{comp} \quad (14)$$

where $\beta_{comp} = 2\pi n_{eff,comp}/\lambda_0$ in the compensation waveguide length L_{comp} of Fig. 4(a).

2) Notch Effects and Reflection Minimization: The waveguides in our devices, such as Fig. 4(b), are 3D in nature, but do not vary in height. Viewed from the top-down, we consider device structures such as ring resonators as 2D waveguide structures composed of three material regions ("layers") as depicted in Fig. 4(b). We denote the guiding structure layer as n_f, and the substrate layers n_s, where $n_f > n_s$. By varying the width of a waveguide, the effective index of the waveguide profile is altered.

Consider the structure depicted in Fig. 5, an "unrolled" representation of the ring structure depicted in Fig. 4(a), and a 2D representation of Fig. 4(b). In place of a single effective index term for a region of the waveguide, the waveguides of the ring are now described in terms of their constituent materials' n_f and n_s refractive indexes, and width and length parameters. We denote the compensation waveguide region as a dielectric "notch" of width w_{comp} and length L_{comp}. This notch is defined as the region of width w_{comp} extracted from the unperturbed waveguide. Therefore, the width of the notch-region *waveguide* is $w - w_{comp}$; the width of the non-compensated regions is w. In terms of the z-dimension, the notch begins at $z = -a$ and ends at $z = a$ for a total length $L_{comp} = 2a$.

The notch changes the properties of the original $n_{eff,\Delta T}$ waveguide, representing a *perturbation* on the waveguide structure. The effect of this perturbation is such that when forward-moving, guided light strikes the notched region, energy is coupled into different modes. These modes can be a combination of: 1) the same mode, but with changes to properties such as phase, 2) inter-mode coupling, if the waveguide supports additional modes, or 3) a combination of (1) and (2) *reflected* into modes of the *backwards* wave.

We analyze Fig. 5 under the assumption that our waveguide is *single-mode.* This simplifies our analysis to consider only

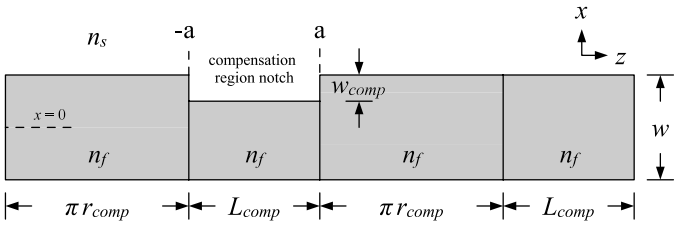

Fig. 5: An unrolled view of a ring resonator

coupling to the forward and backwards traveling waves of the waveguide, A^+ and A^- respectively. Further analysis of perturbations on multimode waveguides can be found in Chapter 10 of [17].

The notch causes a *polarization perturbation* in the waveguide: the product of the change in dielectric constant ($\Delta\varepsilon$) and the electric field of the forward wave (E_y). This perturbation only occurs over the notched region, and therefore:

$$P_{pert} = \begin{cases} \Delta\varepsilon E_y & \text{within notch} \\ 0 & \text{otherwise} \end{cases} \tag{15}$$

$$\Delta\varepsilon = \varepsilon_0 \left(n_s^2 - n_f^2\right) \tag{16}$$

This perturbation causes coupling between modes of the waveguide. In this single-mode waveguide, coupling will occur to the same mode of the forward-traveling wave, and/or reflect into the same mode of the backwards traveling wave. For the forward wave, we have [17]:

$$E(z) = \frac{A^+(-a)}{2} e^{-j(\beta+\kappa)z} \qquad \text{for } -a < z < a \tag{17}$$

where κ is a coupling constant produced by the perturbation. In effect, the perturbation effects a *phase change* (β to $\beta+\kappa$) in the resulting wave — the effect we exploit for the purposes of compensation.

The notch also causes a reflection into the backward wave A^-. The amplitude of this wave, derived in [17], is dependent on the length a:

$$A^-(-a) = \frac{-j\kappa A^+}{\beta} \sin(2\beta a) \tag{18}$$

We wish to minimize reflections, and we note that Eqn. (18) is periodically minimized as a function of a. Therefore, when setting $A^-(-a) = 0$ we have:

$$2\beta a = q\pi \tag{19}$$

$$a = \frac{q\pi}{2\beta} \tag{20}$$

where q is an integer. Given $\beta = 2\pi n_{eff}/\lambda_0$ and $\lambda = \lambda_0/n_{eff}$, Eqn. (20) implies that the length $a = q\lambda/4$. Recall that the notch length $L_{comp} = 2a$. Our reflection-minimizing notch-length is therefore:

$$L_{comp} = \frac{q\pi}{\beta} = \frac{q\lambda}{2} \tag{21}$$

The radius of the curved regions of the template, r_{comp}, is derived by substituting Eqn. (21) into Eqn. (14) and assuming that $\beta = \beta_{\Delta T} \approx \beta_{comp}$:

$$\phi = 2\pi m = \beta\left(2\pi r_{comp} + \frac{q\pi}{\beta}\right) + \beta\frac{q\pi}{\beta} \tag{22}$$

$$= 2\pi(\beta r_{comp} + q) \tag{23}$$

$$r_{comp} = \frac{m-q}{\beta} \tag{24}$$

3) Process Manufacturability: Lithographic processes have resolution limitations that prevent the fabrication of exact widths for notches. We therefore perform additional design space exploration for compensation with respect to process manufacturability. Let $w_{process}$ be the minimum unit width that may be fabricated by the lithographic process. The unit $\Delta\lambda$ shift for the compensation-enabled ring will therefore be defined by:

$$w_{comp}^{unit} = \text{floor}\left(\frac{\Delta w_{comp}}{w_{process}}\right) \cdot w_{process} \tag{25}$$

Though reflections are minimized with respect to notch length, a notch will still cause reflections if it is too deep. Therefore, in order to enable compensation over wide temperature ranges, the compensation region must be lengthened by a multiple of the minimum unit compensation length $\lambda/2$. A benefit of longer compensation lengths is that each $\lambda/2$ subsection of the compensation lengths may be varied independently to effect compensation in a more precise manner. In addition, a longer compensation region reduces the need for deeper notches, which can affect loss. Also, while the ring depicted in Fig. 4(a) only uses a single compensation region, the template ring already includes two possible compensation regions.

5. Methodology and Demonstration for a WDM Ring Resonator

We demonstrate how thermal compensation is achieved by designing a template ring resonator device for a WDM network. This particular resonator structure is designed to filter telecom wavelength $\lambda_0 = 1550$ nm. Each channel of the WDM network utilizes a ring with a specific resonance wavelength λ_0, with sufficient FSR for multiple channels. In this example, we choose an FSR of approximately 15 nm. The system utilizes an SOI ridge waveguide, 400 nm wide and 180 nm in height. For the waveguide profile, we measure $n_g \approx 4.63$ using a mode solver [18]. This leads to a desired ring length:

$$L_{FSR} = \frac{(1550\text{ nm})^2}{4.63 \cdot 15\text{ nm}} \approx 34.6\mu\text{m} \tag{26}$$

Using a mode-solver, we measure an effective index and β for the waveguide profile to be:

$$n_{eff} = 1.9065 \tag{27}$$

$$\beta = \frac{2\pi n_{eff}}{\lambda_0} = 7728317.9/\text{ m} \tag{28}$$

From the value of β we derive a ring length $L \approx L_{FSR}$ that satisfies the resonance condition Eqn. (6):

$$m = \text{floor}\left(\frac{\beta L_{FSR}}{2\pi}\right) = 42 \quad \Rightarrow \quad L = \frac{42 \cdot 2\pi}{\beta} = 34.15\mu\text{m} \tag{29}$$

The total length L enables us to construct a ring resonator structure incorporating a compensation region. We choose a compensation length $L_{comp} = 3\lambda/2$, $3\times$ the minimum notch length ($\lambda/2$), in order to magnify the effects of the perturbation produced by the notch narrowing.

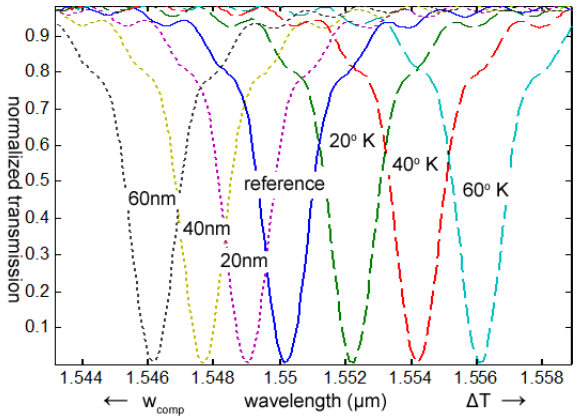

Fig. 6: Wavelength shifts due to changes in ΔT and w_{comp}

We construct and simulate a 3D material representation of our designed ring resonator using an FDTD-type simulator such as Lumerical MODE Solutions or FDTD Solutions [19]. Light is injected into the input of the structure over a range of wavelengths (wavelength sweep), and the transmission response is measured at the through- and drop-ports of the structure. In Fig. 6, we plot the filtering response (measured at the through-port) of the *reference* ring, where $\Delta T = 0, w_{comp} = 0$ nm, reflecting the baseline resonant wavelength for this structure. On the same plot, we also show the wavelength response as a function of: 1) different temperatures ($T = 300^{\circ}K + \Delta T$ for $\Delta T = 0,\ 20,\ 40,\ 60^{\circ}K$), and fixed $w_{comp} = 0$ nm; and 2) *width-narrowing* of the waveguide in the compensation region by a particular amount (w_{comp}), for fixed $\Delta T = 0^{\circ}K$. Observe how temperature increases cause a *positive* resonant wavelength shift. Conversely, narrowing the width of the compensation region's waveguide — by increasing w_{comp}— results in a *negative* wavelength shift. *We can therefore compensate for a static temperature change by narrowing the waveguide of the compensation region.*

The template-ring is compensated for *arbitrary* temperature changes by deriving two sets of sampled values — ΔT *vs* $\Delta\lambda$, and w_{comp} *vs* $\Delta\lambda$ — and coupling these two to derive w_{comp} from ΔT. For the example ring, these tables are presented in Tbl. I. The two tables are derived independently. For ΔT *vs* $\Delta\lambda$, we fix $w_{comp} = 0$ nm, and simulate the ring under different ΔT. Over the device structure, the ΔT is multiplied by each material's thermo-optic coefficient, changing the refractive indexes of the waveguide structures, and effecting wavelength shifts that we sample at the output ports over the range input wavelengths. Likewise, we simulate the ring under different values of notch-narrowing w_{comp}, while fixing $\Delta T = 0$, to determine w_{comp} *vs* $\Delta\lambda$.

From Tbl. I, w_{comp} is derived from an arbitrary ΔT by: 1) interpolating the wavelength shift $\Delta\lambda_{\Delta T}$ using Tbl. I(a); and 2) using $\Delta\lambda_{\Delta T}$ to interpolate a value of w_{comp} from Tbl. I(b). With even a sparse number of sampled points, meaningful thermal compensation can be performed.

For example, if we assume a temperature differential of

TABLE I Wavelength shifts due to ΔT and w_{comp}

ΔT	$\Delta\lambda$
0 ° K	0 nm
10 ° K	1.1035 nm
20 ° K	2.1080 nm
30 ° K	3.0132 nm
40 ° K	4.0202 nm
50 ° K	5.0285 nm
60 ° K	5.9371 nm

(a) ΔT *vs* $\Delta\lambda$

w_{comp}	$\Delta\lambda$
0 nm	0 nm
10 nm	-0.5011 nm
20 nm	-1.1019 nm
30 nm	-1.8023 nm
40 nm	-2.5021 nm
50 nm	-3.2012 nm
60 nm	-3.9995 nm

(b) w_{comp} *vs* $\Delta\lambda$

$\Delta T = 27^{\circ}K$, the predicted interpolated $\Delta\lambda_{\Delta T}$ is calculated as

$$\Delta\lambda_{\Delta T} = 2.1080 \text{ nm} + (3.0132 \text{ nm} - 2.1080 \text{ nm})\frac{(27-20)^{\circ}K}{(30-20)^{\circ}K}$$
$$= 2.7417 \text{ nm} \quad (30)$$

We compensate for this positive wavelength shift with an equal negative wavelength shift by interpolating w_{comp} from Tbl. I(b):

$$w_{comp} = 40 \text{ nm} + (50-40) \text{ nm}\frac{(2.7417+2.5021) \text{ nm}}{(-3.2012+2.5021) \text{ nm}}$$
$$= 43.4265 \text{ nm} \quad (31)$$

This yields $w_{comp} \approx 40$ nm (very feasible in contemporary lithography processes). The wavelength response comparing the compensated system with the reference system is depicted in Fig. 7. By inspection, the two response curves are in very close agreement.

This example and supporting methodology demonstrate that we can compensate for temperature-induced resonant-wavelength shifts in ring-resonators by varying the width of waveguides in subsections of the ring. The benefit of this approach is that a single template can be constructed that accommodates a wide range of temperature variations, while remaining relatively precise. The example also only uses one of the possible compensation regions, and the precision of compensation could be further improved by independently varying subsections of each compensation region.

The ring resonator template and compensation parameters are generated using automated scripts in conjunction with a

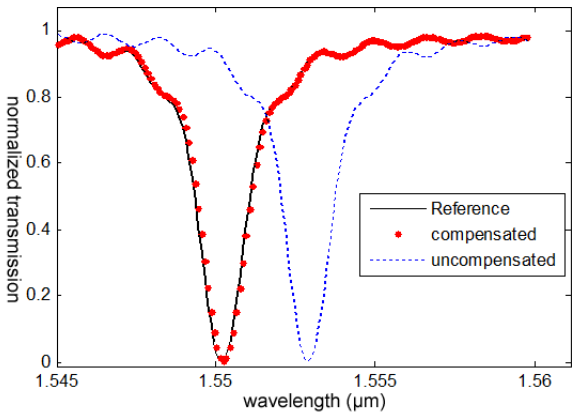

Fig. 7: Compensation for $\Delta T = 27^{\circ}K$ with $w_{comp} = 40$ nm vs. unaffected reference ring

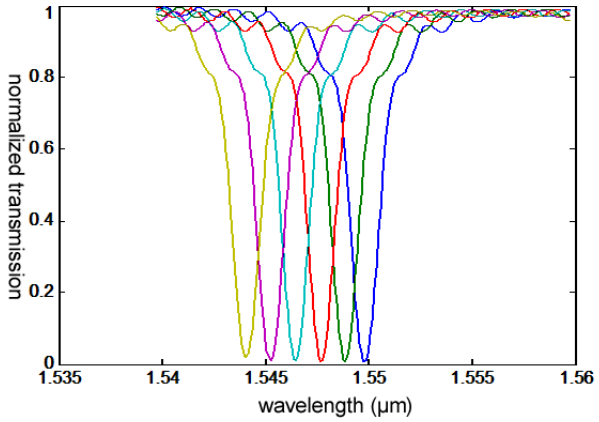

(a) Compensation range for $L_{comp} = 5 \cdot \lambda/2$

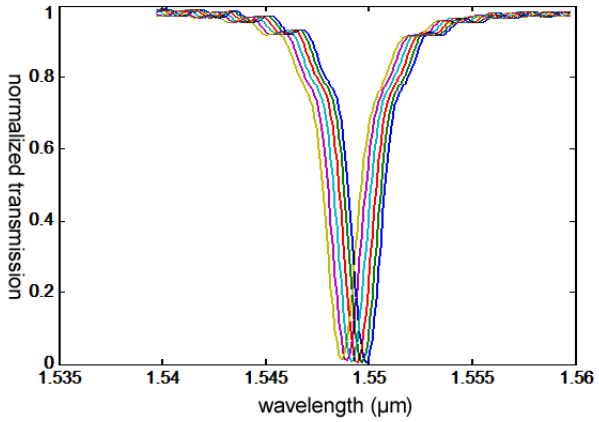

(b) Compensation range for $L_{comp} = 1 \cdot \lambda/2$

Fig. 8: Effect of compensation region length on compensation range

parameterized FDTD simulation analysis. We also apply the automated technique to varying compensation region lengths using the same base ring resonator parameters. In the the experiments depicted in Fig. 8, for fixed $\Delta T = 0$, we plot the response for different $w_{comp} = 60$ nm$\ldots 10$ nm. As observed, the range of compensation is proportional to the length of the compensation region. A larger L_{comp} can be used for shifting λ_0 over a wider range.

6. Conclusion

Thermal interactions of electronic and optical systems present many challenges to the integration of optical network fabrics. Electronic switching may create temperature-hotspots that will interact with the optical substrate, producing thermal gradients. Photonic ring resonators — key components of on-chip optical WDM networks — are particularly susceptible to thermal variations. Thermal compensation is required, often in the form of active tuning such as micro-heaters and DC biasing. However, such methods are costly in terms of area and power, and tuning range is limited.

This paper has detailed a *static*-compensation approach based on thermal-aware, physical (re)synthesis of ring resonators. Our technique complements active tuning methods by pre-compensating for known thermal variation. We present a template-based methodology exploiting perturbation theory applied to waveguide dimension changes. An automated approach is demonstrated, analyzing simulated data over an uncompensated ring to derive redesign parameters for thermal compensation. The effect of this resynthesis is that less active-tuning is required for ensuring an operational optical communications network. This, in turn, saves power required for integration into opto-electronic hybrid systems.

References

[1] R. K. Dokania and A. B. Apsel, "Analysis of challenges for on-chip optical interconnects", *in Proc. 19th ACM Great Lakes Symp. VLSI*, GLSVLSI '09, pp. 275–280, New York, NY, USA, 2009. ACM.

[2] W. Bogaerts et al., "Silicon microring resonators", *Laser & Photonics Reviews*, vol. 6, pp. 47–73, 2012.

[3] S. Manipatruni, R. K. Dokania, B. Schmidt, N. Sherwood-Droz, C. B. Poitras, A. B. Apsel, and M. Lipson, "Wide temperature range operation of micrometer-scale silicon electro-optic modulators", *Opt. Lett.*, vol. 33, pp. 2185–2187, Oct. 2008.

[4] IBM Research, "Silicon Integrated Nanophotonics Technology: from the Lab to the Fab", http://www.research.ibm.com/photonics, 2012.

[5] F. Gan, T. Barwicz, M.A. Popovic, M.S. Dahlem, C.W. Holzwarth, P. T. Rakich, H.I. Smith, E.P. Ippen, and F.X. Kartner, "Maximizing the thermo-optic tuning range of silicon photonic structures", *in Photonics in Switching*, pp. 67–68, 2007.

[6] C. Shih, Z. Zeng, and C. Shiuh, "Extinction ratio compensation by free carrier injection for a MOS-capacitor microring optical modulator subjected to temperature drifting", *in Proc. Conf. Lasers Electro Optics / Pacific Rim Conf. Lasers and Electro-Optics*, pp. 1–2, Aug. 2009.

[7] A. Qouneh, Z. Li, M. Joshi, W. Zhang, X. Fu, and T. Li, "Aurora: A thermally resilient photonic network-on-chip architecture", *in Computer Design (ICCD), 2012 IEEE 30th International Conference on*, pp. 379–386, 2012.

[8] I. Christiaens, D. Van Thourhout, and R. Baets, "Low-power thermo-optic tuning of vertically coupled microring resonators", *Electron. Lett.*, vol. 40, pp. 560–561, Apr. 2004.

[9] P. Li, L.T. Pileggi, M. Asheghi, and R. Chandra, "Efficient full-chip thermal modeling and analysis", *in Proc. IEEE/ACM Int. Conf. Comput.-Aided Design*, pp. 319–326, 2004.

[10] A.V. Krishnamoorthy, R. Ho, X. Zheng, H. Schwetman, J. Lexau, P. Koka, G. Li, I. Shubin, and J.E. Cunningham, "Computer Systems Based on Silicon Photonic Interconnects", *Proc. IEEE*, vol. 97, pp. 1337–1361, Jul. 2009.

[11] Y. Zheng, P. Lisherness, M. Gao, J. Bovington, K. Cheng, H. Wang, and S. Yang, "Power-efficient calibration and reconfiguration for optical network-on-chip", *J. Opt. Commun. Netw.*, vol. 4, pp. 955–966, Dec. 2012.

[12] D. Ding, B. Yu, and D. Pan, "GLOW: A global router for low-power thermal-reliable interconnect synthesis using photonic wavelength multiplexing", *in Proc. Asia and South Pacific Design Autom. Conf.*, pp. 621–626, Feb. 2012.

[13] J. Schrauwen, D. Thourhout, and R. Baets, "Trimming of silicon ring resonator by electron beam induced compaction and strain", *Opt. Express*, vol. 16, pp. 3738–3743, Mar. 2008.

[14] S. Lambert, W. D. Cort, J. Beeckman, K. Neyts, and R. Baets, "Trimming of silicon-on-insulator ring resonators with a polymerizable liquid crystal cladding", *Opt. Lett.*, vol. 37, pp. 1475–1477, May 2012.

[15] J. Teng, P. Dumon, W. Bogaerts, H. Zhang, X. Jian, M. Zhao, G. Morthier, and R. Baets, "Athermal SOI ring resonators by overlaying a polymer cladding on narrowed waveguides", *in Proc. 6th IEEE Int. Conf. Group IV Photon.*, pp. 77–79, 2009.

[16] K. Hill and G. Meltz, "Fiber Bragg grating technology fundamentals and overview", *J. Lightw. Technol.*, vol. 15, pp. 1263–1276, 1997.

[17] C. Pollock and M. Lipson, *Integrated Photonics*, Kluwer Academic Publishers, Norwell, MA, USA, 2003.

[18] E. Dulkeith, F. Xia, L. Schares, W. M. J. Green, and Y. A. Vlasov, "Group index and group velocity dispersion in silicon-on-insulator photonic wires", *Opt. Express*, vol. 14, pp. 3853–3863, May 2006.

[19] Lumerical Solutions, Inc., *Lumerical Photonics CAD Suite*, http://www.lumerical.com.